

Supercomputer Simulation Study of the Convergence of Iterative Methods for Solving Inverse Problems of 3D Acoustic Tomography with the Data on a Cylindrical Surface

Sergey Romanov^[0000–0001–7882–2061]

Lomonosov Moscow State University, Moscow, Russia
romanov60@gmail.com

Abstract. This paper is dedicated to developing effective methods of 3D acoustic tomography. The inverse problem of acoustic tomography is formulated as a coefficient inverse problem for a hyperbolic equation where the speed of sound and the absorption factor in three-dimensional space are unknown. Substantial difficulties in solving this inverse problem are due to its nonlinear nature. A method which uses short sounding pulses of two different central frequencies is proposed. The method employs an iterative parallel gradient-based minimization algorithm at the higher frequency with the initial approximation of unknown coefficients obtained by solving the inverse problem at the lower frequency. The efficiency of the proposed method is illustrated via a model problem. In the model problem an easy to implement 3D tomographic scheme is used with the data specified at a cylindrical surface. The developed algorithms can be efficiently parallelized using GPU clusters. Computer simulations show that a GPU cluster capable of performing 3D image reconstruction within reasonable time.

Keywords: Ultrasound tomography · Medical imaging · Inverse problem · Gradient method.

1 Introduction

This paper is dedicated to methods of acoustic tomography, or, to be more specific, to ultrasound tomography used for imaging of soft tissues in medicine [22, 12, 23]. Differential diagnosis of breast cancer is one of the most important problems in modern medicine. Ultrasonic tomography could be the most promising method for regular mammographic screening.

However, currently existing ultrasonic devices are not tomographic. The reflectivity images obtained by these devices reveal only the contours of tissue irregularities and do not make it possible to characterize the tissues with sufficient resolution. Hence developing high-resolution ultrasound tomographs for imaging of soft tissues is very important task.

The most interesting results in ultrasound tomography are associated with the development of methods for solving problems of 3D wave tomography in

terms of mathematical models incorporating both diffraction and absorption effects. Breakthrough results in mathematical methods for solving inverse problems are due to the possibility of directly computing the gradient of the residual functional between the computed and experimental data at the detectors [2, 16, 17, 13, 11, 8]. Detectors are placed at a cylindrical surface surrounding the object studied. This is the underlying approach of the methods used in this paper.

One approach to ultrasound tomography involves using simplified linearized models [22, 20, 24]. However, a linearized model can provide only a rough characterization of tissues [21].

The development of numerical methods for solving direct and inverse problems of wave tomography is a challenging computational task [3]. We solve the direct problem using finite difference approximation of hyperbolic-type differential equations. To solve inverse problems, we use iterative parallel algorithms based on direct computation of the gradient of the residual functional. To compute the gradient, we solve the conjugate problem in reverse time. The amount of input data and the number of unknowns in the inverse 3D problem exceed 1 Gb and 100Mb, respectively. The algorithms are implemented on a supercomputer.

Because of the nonlinearity of the inverse problems of wave tomography the residual functional is not convex, and this presents one of the main mathematical challenges. As a consequence, gradient-based methods that minimize the residual functional converge to some local minimum rather than the global minimum of the functional. There are various approaches to find the global minimum of a non-convex functional. Attempts were made to construct "global" methods [13, 2, 14] to solve inverse problems.

In this paper, the dual-frequency method is proposed for finding approximate solutions of 3D coefficient inverse problems in acoustic tomography. The dual-frequency method extends the domain of convergence of gradient-based algorithms. This method can be applied primarily to ultrasound tomography. The efficiency of the proposed method is illustrated via model problems. The developed algorithms are easily parallelized using supercomputers and GPU-clusters [7, 18]. Computer simulations show that a GPU cluster capable of performing 3D image reconstruction within reasonable time.

2 Formulation and Solution Methods of the Inverse Problem of 3D Acoustic Tomography

The aim of acoustic tomography is to reconstruct the internal structure of the object using measurements of the acoustic pressure $u(\mathbf{r}, t)$ obtained on some surface surrounding the object. Fig. 1 shows the scheme of a 3D acoustic tomographic examination where the measurements are taken on a cylindrical surface. The emitters of sounding pulses are located on the same cylindrical surface. This tomographic scheme can be used for ultrasonic mammography.

The formulation of the inverse problem of ultrasound tomography with the data specified at a cylindrical surface is a novel approach. The peculiarity of the algorithms developed for solving the inverse problem considered is that numerical

methods use Cartesian coordinate system, making it necessary to minimize errors of the interpolation of the computed wave field onto the cylindrical surface. The tomographic scheme with the data specified at a cylindrical surface is easy to implement in physical experiments.

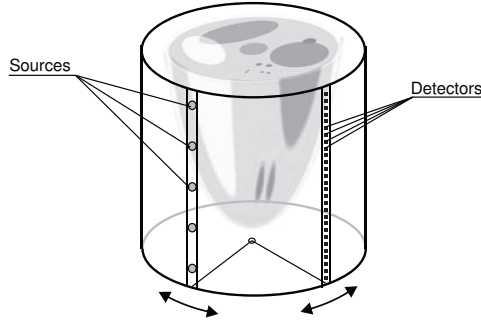


Fig. 1. The scheme of a tomographic examination.

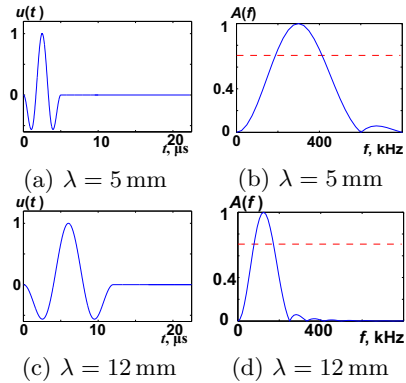


Fig. 2. Sounding pulse for different wavelengths: waveform (a,c) ; frequency spectrum (b,d).

The scalar wave model is used to describe the wave propagation process. This model also takes into account such important factor as ultrasound absorption in the medium. The initial pulse emitted by a point source was calculated using the formula $u(x) = \sin(2\pi x/(3\lambda)) \cdot \sin(6\pi x/(3\lambda))$, $x \leq 1.5\lambda$. Fig. 2a,b shows the waveform and the frequency spectrum of a pulse with a wavelength of 5 mm, Fig. 2c,d shows the waveform and the frequency spectrum of a pulse with a wavelength of 12 mm. The bandwidth of these pulses at -3dB level (indicated by a dotted line) is approximately 65% of the central frequency.

The simplest absorption model is used in this paper [9]. The inverse problem of ultrasound tomography can then be formulated as a coefficient inverse problem of reconstructing the unknown coefficients $c(\mathbf{r})$ and $a(\mathbf{r})$ in the wave equation, given the measurements of the acoustic pressure on the surface S made with different positions \mathbf{q} of the sources:

$$c(\mathbf{r})u_{tt}(\mathbf{r}, t) + a(\mathbf{r})u_t(\mathbf{r}, t) - \Delta u(\mathbf{r}, t) = \delta(\mathbf{r} - \mathbf{q}) \cdot f(t); \quad (1)$$

$$u(\mathbf{r}, t)|_{t=0} = 0, \quad u_t(\mathbf{r}, t)|_{t=0} = 0, \quad \partial_n u(\mathbf{r}, t)|_{ST} = p(\mathbf{r}, t). \quad (2)$$

Here $c(\mathbf{r}) = 1/v^2(\mathbf{r})$, where $v(\mathbf{r})$ is the speed of sound in the medium; $\mathbf{r} \in \mathbb{R}^N$ ($N = 3$), the position of the point in space; u , the acoustic pressure; Δ , the Laplace operator with respect to the variable \mathbf{r} . The function $f(t)$ describes the sounding pulse generated by a point source at \mathbf{q} ; $\partial_n u(\mathbf{r}, t)|_{ST}$ is the derivative along the normal to the surface S in the range $(\mathbf{r}, t) \in S \times (0, T)$, where T is the duration of the measurement. The function $p(\mathbf{r}, t)$ is known, and $a(\mathbf{r})$ is the

4 S. Romanov

absorption factor. Formulas (2) represent the initial conditions and the Neumann conditions at the boundary of the computational domain.

It is assumed that inhomogeneity of the medium is caused by variations of the sound speed and absorption factor. Outside of the region studied the absorption factor is equal to zero, $a(\mathbf{r}) = 0$, and the speed of sound is known and equal to $v_0 = \text{const}$. This simple model of wave propagation with absorption (1) can be used to describe ultrasound waves in soft tissues.

The inverse problem is formulated as the problem of minimizing the residual functional $\Phi(c(\mathbf{r}), a(\mathbf{r}))$ with respect to its argument (c, a) :

$$\Phi(u(c, a)) = \frac{1}{2} \int_0^T \int_S (u(\mathbf{s}, t) - U(\mathbf{s}, t))^2 d\mathbf{s} dt. \quad (3)$$

Here $U(\mathbf{s}, t)$ is the acoustic pressure measured at the boundary S for the duration $(0, T)$, and $u(\mathbf{s}, t)$ is the solution of the direct problem (1)–(2) for the given $c(\mathbf{r}) = 1/v^2(\mathbf{r})$ and $a(\mathbf{r})$. For multiple ultrasound sources the total value of the residual functional is the sum of the residuals (3) for each source.

Formulas for the gradient $\Phi'(c, a)$ of the residual functional for two- and three-dimensional inverse problems in various formulations were derived in the works [17, 16, 2]. A strict mathematical derivation of the gradient for the inverse problem (1)–(2) using a model that accounts for the diffraction and absorption effects was presented in the papers [8, 6, 10].

The gradient $\Phi'(u(c, a)) = \{\Phi'_c(u), \Phi'_a(u)\}$ of the functional (3) with respect to the variation $\{dc, da\}$ of the sound speed and absorption factor has the following form:

$$\Phi'_c(u(c)) = \int_0^T w_t(\mathbf{r}, t) u_t(\mathbf{r}, t) dt, \quad \Phi'_a(u(a)) = \int_0^T w_t(\mathbf{r}, t) u(\mathbf{r}, t) dt. \quad (4)$$

Here $u(\mathbf{r}, t)$ is the solution of the main problem (1)–(2), and $w(\mathbf{r}, t)$ is the solution of the “conjugate” problem for the given $c(\mathbf{r})$, $a(\mathbf{r})$, and $u(\mathbf{r}, t)$:

$$w_{tt}(\mathbf{r}, t) - a(\mathbf{r})w_t(\mathbf{r}, t) - \Delta w(\mathbf{r}, t) = 0; \quad (5)$$

$$w(\mathbf{r}, t = T) = 0, \quad w_t(\mathbf{r}, t = T) = 0, \quad \partial_n w|_{ST} = u|_{ST} - U. \quad (6)$$

The boundary condition $\partial_n w|_{ST} = 0$ is applied at the part of the boundary S where there are no detectors. To compute the gradient (4), the direct problem (1)–(2) and the “conjugate” problem (5)–(6) must be solved.

Given the representation of the gradient (4), various iterative algorithms can be used to minimize the residual functional. One of the simplest algorithms is the steepest descent method.

The finite difference time-domain (FDTD) method on a uniform grid is used to solve the three-dimensional equations (1)–(2) and (5)–(6). The grid step h and time step τ are related by the Courant stability condition $\sqrt{3} \cdot c^{-0.5} \tau < h$, where

$c^{-0.5} = v$ is the speed of sound. The following second-order finite difference scheme is used to approximate equation (1):

$$c_{ijl} \frac{u_{ijl}^{k+1} - 2u_{ijl}^k + u_{ijl}^{k-1}}{\tau^2} + a_{ijl} \frac{u_{ijl}^{k+1} - u_{ijl}^{k-1}}{\tau} - \frac{\Delta u_{ijl}^k}{h^2} = 0 \quad (7)$$

Here $u_{ijl}^k = u(x_i, y_j, z_l, t_k)$ is the value of $u(\mathbf{r}, t)$ at the point (i, j, l) at the time step k ; c_{ijl} and a_{ijl} are the values of $c(\mathbf{r})$ and $a(\mathbf{r})$ at (i, j, l) . Δ is the discrete Laplacian, which is computed using the formula:

$$\Delta u_{i_0, j_0, l_0}^k = \sum_{i=i_0-1}^{i_0+1} \sum_{j=j_0-1}^{j_0+1} \sum_{k=k_0-1}^{k_0+1} b_{ijl} u_{ijl}^k. \text{ The coefficients } b_{ijl} \text{ are provided,}$$

for example, in the paper [15]. A similar finite difference scheme is used to solve equations (5)–(6) in reverse time. The iterative process for solving the inverse problem numerically is described in [4].

3 GPU-Implementation of the Explicit Finite-Difference Algorithm for 3D Ultrasound Tomography

The algorithm for solving the inverse problem of ultrasound tomography is highly data parallelizable [1, 5]. The values at all the grid points are computed at all time steps by the same formula both in the “direct” (1)–(2) and “conjugate” (5)–(6) problem and are independent of each other. Such algorithms can be efficiently parallelized on SIMD/SPMD-architectures.

A typical size of the 3D problem is $\approx 400^3$, while the number of parallel threads supported by a GPU device is on the order of 10000. Therefore, the algorithm processes the 3D data array sequentially along the Z-axis (z-marching method), as shown in Fig. 3. Sequential memory accesses are efficiently and automatically cached by modern GPUs and can be rapidly loaded into GPU registers.

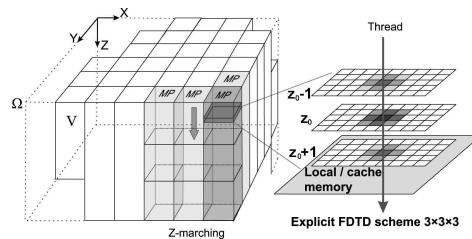


Fig. 3. GPU-implementation of the explicit 3D algorithm.

In the Z-marching FDTD implementation, at each step along the Z-axis the next layer ($z = z_0 + 1$) is loaded into the registers, and the results for the current computed layer ($z = z_0$) are saved to the global memory. The process is then

6 S. Romanov

repeated for the next value of $z = z + 1$. The data for the current horizontal layer reside in the cache and can be read by all threads with no performance penalty. Each thread computes the results for points (x, y, z) , where x and y are fixed, and the Z range includes several dozen points. The highest performance on the devices tested is achieved if each 32×4 -thread block processes a $32 \times 4 \times 32$ -point volume of data.

Nearly constant speed of sound, which differs from the speed of sound in water by no more than 10%, is a specific feature of soft tissue tomography. Taking into account this feature, the algorithm dynamically adjusts the computational domain and processes only the volume where the waves emitted by the source can be present. This volume is designated as V in Fig. 3 and is the intersection of the cubic computational domain Ω and the sphere of radius $Vmax \cdot t$ centered at the source. Here $Vmax$ is the maximum sound speed in soft tissues, and t is the current simulation time. The set of blocks that intersect with the domain V is precomputed, and only these blocks are launched at a given simulation time t . Dynamic computational domain adjustment increases the performance by 30–40%.

4 Convergence of the Iterative Algorithms Used to Solve the Inverse Problem

The inverse problem of wave tomography in the proposed formulation is a nonlinear coefficient inverse problem. The residual functional of a nonlinear problem is typically non-convex, and thus it has local minima. In this paper, we investigate how the behavior of the residual functional depends on physical parameters, such as the wavelengths of sounding pulses. The ultimate goal of this work is to develop algorithms that make it possible to obtain an approximate solution of the coefficient inverse problem using some initial approximation.

A simple one-dimensional model problem is presented to illustrate how the wavelength of sounding pulses affects the convergence of gradient minimization algorithms. The ultrasound pulse propagates through one-dimensional medium with the speed of sound defined by the relations $c(x) = \bar{c}$ for $|x| \leq r$, $c(x) = c_0$ for $|x| > r$. Fig. 4 shows the scheme of propagation of sounding pulses emitted by the source S. The sounding pulse 1 in Fig. 4a propagates from the source S at a speed of c_0 . In the inhomogeneous region $|x| < r$, the pulse propagates at a speed of \bar{c} . Should there be no inhomogeneity, the sounding pulse in Fig. 4a would arrive at position 2 at some time T . The difference between \bar{c} and c_0 in the inhomogeneous region causes the pulse to shift and arrive at position 3 at the time T . The detector D registers the acoustic pressure as a function of time $U(t)$. Assuming that the position of the inhomogeneity $|x| < r$ is known, the inverse problem is to determine the unknown speed of sound \bar{c} in the region $|x| < r$, given the waveform $U(t)$ received by the detector.

We introduce the residual functional $\Phi(c) = \|U(t) - u(c, t)\|^2$, where $u(c, t)$ is the numerically simulated pulse at the detector position D computed assuming that the speed of sound in the inhomogeneous region is equal to c . The point

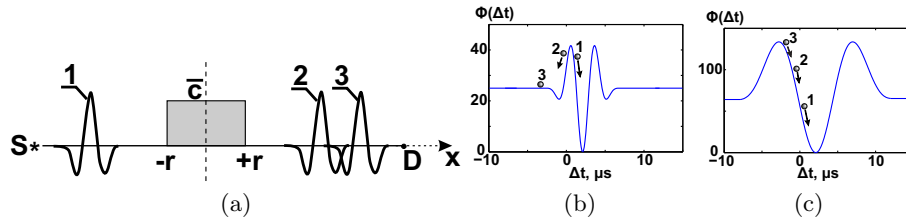


Fig. 4. Positions of sounding pulses with the inhomogeneity present and with the inhomogeneity absent (a). Plots of the residual functional for $\lambda = 5$ mm (b) and for $\lambda = 12$ mm (c).

of the global minimum of functional $\Phi(c)$ is the exact solution of the inverse problem. The value of the functional at this point is 0.

Let us denote the difference in pulse arrival times caused by the difference between c and c_0 as $\Delta t(c) = 2(r/c_0 - r/c)$. Fig. 4b,c shows the plots of the residual functional $\Phi(\Delta t) = \|U(t) - u(c(\Delta t), t)\|^2$ as a function of the pulse arrival time difference Δt for different wavelengths. Here $\|U(t) - u(c(\Delta t), t)\|^2 = \int_{t=0}^T (U(t) - u(c(\Delta t), t))^2 dt$.

Fig. 4b shows that for a shorter wavelength the iterative process of minimizing the residual functional converges to the global minimum from the initial approximation 1 and does not converge from initial approximations 2 and 3. For a longer wavelength the iterative process converges to the global minimum from any initial approximation 1,2 or 3, as shown in Fig. 4c.

Hence the use of sounding pulses of at least two different central wavelengths λ_1 and λ_2 , $\lambda_1 > \lambda_2$ seems to be a promising approach for expanding the domain of convergence of the iterative method. First, a number of iterations of the gradient method is performed using the longer wavelength λ_1 . The resulting approximate solution falls into the domain of convergence of the iterative process for the shorter wavelength λ_2 . Then the residual functional is minimized via the gradient method using the wavelength λ_2 . This idea forms the basis of the proposed dual-frequency method used to solve the problem of acoustic tomography.

In reality, the inverse problem is three-dimensional. Outside of the object, the speed of sound is $c(\mathbf{r}) = const = c_0$, $\mathbf{r} \in \mathbb{R}^3$. The object is insonified using the pulses emitted by sources S . Detectors D register the acoustic pressure $U(t)$ as a function of time. It turns out that the properties of the residual functional in the three-dimensional case are quite similar to the one-dimensional example described above.

Fig. 5 shows the positions of wave fronts at some time T . The central wavelengths of the pulses are $\lambda = 5$ mm and $\lambda = 12$ mm for Fig. 5a and Fig. 5b, respectively. The dotted line 1 in Figures 5a, 5b shows the position of the wave front at time T in a homogeneous medium, assuming that the object is absent. It corresponds to the pressure field $u(\mathbf{r}, T)$ computed at the initial iteration, according to the formulation of the inverse problem (3). The dotted line 2 shows

8 S. Romanov

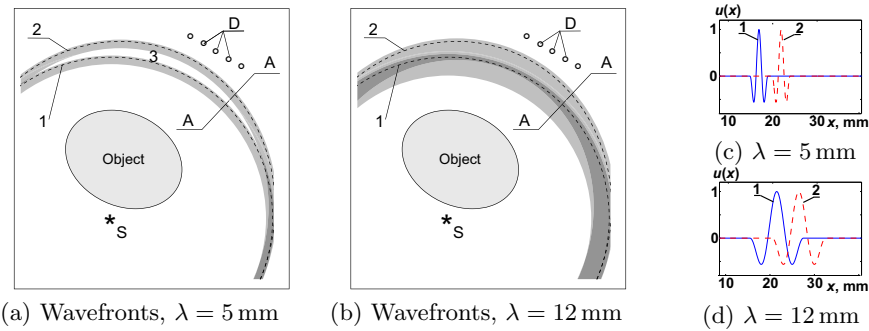


Fig. 5. Wavefront of the sounding waves (a,b) and cross-sections of the pressure field along the A–A line (c,d) for different wavelengths.

the position of the wave front that has passed through the object. It corresponds to the measured pressure field $U(\mathbf{r}, T)$. The gray area in Figures 5a, 5b corresponds to the pulse width. A cross-section of the pressure field along the A–A line would be similar to the one-dimensional case.

Fig. 5c,d shows the pressure fields along the A–A line with the object present and with the object absent, for $\lambda = 5$ mm (Fig. 5c) and for $\lambda = 12$ mm (Fig. 5d) respectively. The number “1” denotes the simulated wave $u(\mathbf{r}, T)$ propagating in a homogeneous medium at a velocity of c_0 . The number “2” denotes the wave that has passed through the object.

The pulses with $\lambda = 5$ mm do not overlap, and there exists a region 3 between the wave fronts, where $u \approx 0$ and $U \approx 0$. Similarly to the one-dimensional case, the gradient of the residual functional between the measured wave 2 and the simulated wave 1 in this case is equal to zero. Therefore, the iterative gradient method used to minimize the residual functional does not converge. If the wavelength is increased to $\lambda = 12$ mm, the waves 1 and 2 overlap. Then the initial approximation c_0 falls into the domain of convergence of the iterative process.

Actual acoustic tomography experiments involve dozens of source positions and thousands of detector positions. The residual functional (3) is the sum of the residuals computed for every source-detector pair.

These examples show that choosing an initial approximation is an important issue, which affects the convergence of the iterative gradient-based method. If there is no prior information about the structure of the inhomogeneity, the known sound speed c_0 of the surrounding medium can be used as an initial approximation. This approach is natural in ultrasonic mammography, where the sound speed difference between soft tissues and water is less than 10%.

These examples lead to the following conclusions. The following dual-frequency method to find an approximate solution of the inverse problem can be used to extend the domain of convergence of the gradient method. The measurements are performed using sounding pulses with two different central frequencies f_1 and f_2 , $f_1 < f_2$. The frequencies f_1 and f_2 should differ by a factor of 2 to 3. An approximate solution is found by minimizing the residual functional at the

lower frequency f_1 . The frequency f_1 is chosen low enough so that an initial approximation of c_0 is sufficient for the gradient descent method to converge. The obtained solution is used as an initial approximation for the iterative process that minimizes the residual functional at the higher frequency f_2 .

5 Numerical Simulations

Fig. 1 shows the scheme of the numerical experiment for the three-dimensional problem of ultrasound tomography. The sounding pulses are emitted by 24 sources according to the scheme of the experiment in which a rotating mount with 4 ultrasound transducers through 6 positions in 60-degree intervals. The detectors are located on a cylindrical surface with a diameter and height of 130 mm. The simulated detector array has a pitch of 2 mm. The finite difference grid size is $448 \times 448 \times 448$ points. The total durations of sounding pulses are $5 \mu s$ and $12 \mu s$, which corresponds to the central wavelengths of 5 mm and 12 mm.

The numerical experiment consisted of solving the direct problem of wave propagation and computing the acoustic pressure $U(\mathbf{s}, t)$ at the detectors located at points \mathbf{s} of a cylindrical surface, and then using the data obtained, $U(\mathbf{s}, t)$, to solve the inverse problem and reconstruct the speed of sound $c(\mathbf{r})$ and the absorption factor $a(\mathbf{r})$.

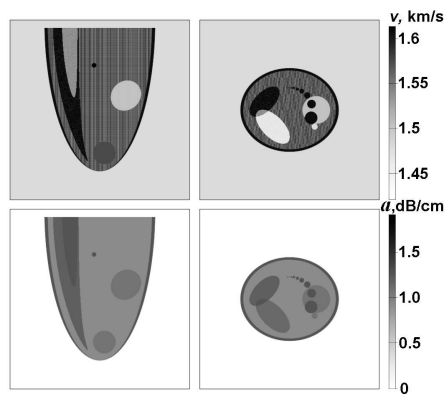


Fig. 6. Simulated phantom: speed of sound $c(\mathbf{r})$ and absorption factor $a(\mathbf{r})$.

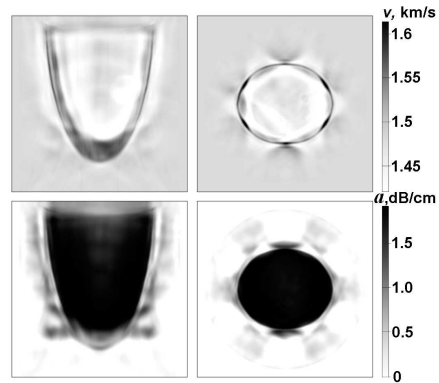


Fig. 7. Images $\{c, a\}_{loc}$ reconstructed using $\lambda = 5$ mm and the initial approximation $c_0 = const, a_0 = 0$.

Fig. 6 shows the cross-sections of the sound speed $c(\mathbf{r})$ and absorption factor $a(\mathbf{r})$ in the simulated phantom, for which the direct problem was solved. The acoustic parameters of the phantom were chosen to match typical parameters of soft tissues: the speed of sound ranges from 1400 to 1600 $m \cdot s^{-1}$, the absorption factor ranges from 0 (in water) to 1.2 dB/cm. The ambient sound speed

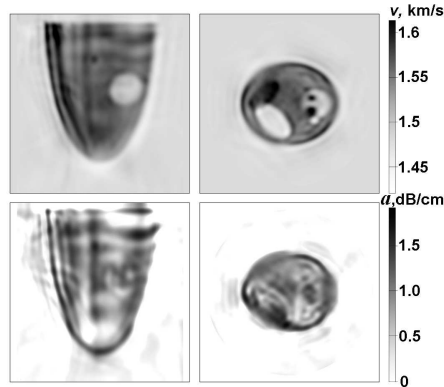


Fig. 8. Images $\{c_1, a_1\}$ reconstructed using $\lambda = 12$ mm and the initial approximation $c_0 = const, a_0 = 0$.

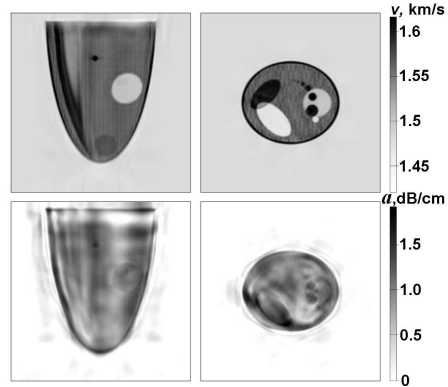


Fig. 9. Images $\{c_2, a_2\}$ reconstructed using $\lambda = 5$ mm and the initial approximation $\{c_1, a_1\}$ shown in Fig. 8.

c_0 is $1500 \text{ m}\cdot\text{s}^{-1}$. The wave propagation model (1)–(2) assumes the frequency-independent absorption law.

The phantom contains inclusions ranging in size from 2 to 10 mm with various sound speeds c and absorption factors a , and an area filled with an anisotropic texture with spatial frequencies ranging from 0.5 to 3 mm^{-1} . The exact values of the sound speed and absorption factor of the phantom are denoted as $\{\bar{c}, \bar{a}\}$.

Figures 7, 8, and 9 show the reconstructed images of the sound speed $c(\mathbf{r})$ and absorption factor $a(\mathbf{r})$ obtained via numerical simulations. In the first numerical simulation we attempt to reconstruct the coefficients $c(\mathbf{r})$ and $a(\mathbf{r})$ inside the simulated object using the gradient method with an initial approximation of $c_0 = const, a_0 = 0$. The central wavelength of the sounding pulses was set to 5 mm. Fig. 7 shows the result of this numerical simulation. The images in Fig. 7 were obtained at the 100th iteration of the gradient method, after which the iterative process stopped at the local minimum of the residual functional. The obtained sound speed and absorption factor are denoted as $\{c, a\}_{loc}$. The global minimum of the functional corresponds to the exact image (Fig. 6) and the coefficients $\{\bar{c}, \bar{a}\}$. The value of the functional $\Phi(\bar{c}, \bar{a}) = 0$.

In the second numerical experiment the wavelength of the sounding pulses was increased to 12 mm for the initial approximation c_0 to become close enough to the global minimum of the residual functional. Fig. 8 shows the $c(\mathbf{r})$ and $a(\mathbf{r})$ images obtained via the gradient method with an initial approximation of $c_0 = const, a_0 = 0$ and $\lambda = 12$ mm. This image has a very low spatial resolution. The approximate solution $c(\mathbf{r})$ and $a(\mathbf{r})$ obtained in the experiment with $\lambda = 12$ mm is denoted as $\{c_1, a_1\}$.

Fig. 9 shows the approximate solution $\{c_2, a_2\}$ obtained in this experiment via the gradient method using the initial approximation $\{c_1, a_1\}$. The reconstructed sound speed image $c_2(\mathbf{r})$ is close to the exact image of the phantom (Fig. 6).

We computed the values of the functional on the linear manifold containing the exact solution $\{\bar{c}, \bar{a}\}$ and the obtained approximate solution $\{c, a\}_{loc}$. This manifold consists of the elements $X_\alpha = (1 - \alpha) \cdot \{c, a\}_{loc} + \alpha \cdot \{\bar{c}, \bar{a}\}$.

Fig. 10 shows the plot the residual functional $\Phi(\alpha)$ over this linear manifold. Like in the 1D example, in the 3D case the plot of the residual functional resembles the waveform of the sounding pulse. The approximate solution $\{c, a\}_{loc}$ is at a local minimum of the functional ($\alpha = 0$).

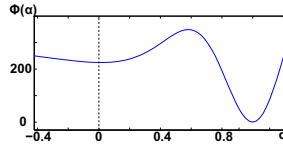


Fig. 10. Plot of the residual functional $\Phi(\alpha)$, $\lambda = 5$ mm.

Thus, we showed that a two-stage method of tomographic reconstruction allows us to expand the domain of convergence of the gradient method and to obtain a high-resolution sound speed image using zero initial approximation.

We performed our simulations on the Lomonosov supercomputer of Moscow State University [19] equipped with NVIDIA Tesla X2070 GPU devices, two devices per computing node, and QDR Infiniband 4x (40 GBit/s) interconnect network. Single-precision floating point arithmetic was used in 3D computations. The number of GPU devices employed was equal to that of ultrasound sources (24). The 3D image was reconstructed in approximately two hours.

6 Conclusions

This paper presents a method for ultrasound tomography imaging of soft tissues for medical and biological research. Efficient algorithms have been developed for solving inverse problems of low-frequency tomography on a supercomputer. The most important issue in ultrasound tomography data interpretation is the nonlinearity of the coefficient inverse problem.

Our study showed that the lower is the sounding frequency the broader is the convergence domain of iterative processes. A method is proposed that involves the use of multiple frequency bands. The method employs an iterative gradient-based minimization algorithm at the higher frequency with the initial approximation of unknown coefficients obtained by solving the inverse problem at the lower frequency.

The numerical simulations were performed using the setup where acoustic pressure is measured on a cylindrical surface. Such a setup can be easily implemented using rotating vertical transducer arrays.

The methods developed can be used to design tomographic devices for differential diagnosis of breast cancer. The iterative algorithms used to solve the

inverse problems of wave tomography can be efficiently parallelized using GPU clusters. The increasing performance of modern GPU clusters makes them a suitable computing device for ultrasound tomographs currently being developed.

Acknowledgement This work was supported by Russian Science Foundation [grant number 17-11-01065]. The research is carried out at Lomonosov Moscow State University. The research is carried out using the equipment of the shared research facilities of HPC computing resources at Lomonosov Moscow State University.

References

1. Bazulin, E.G., Goncharsky, A.V., Romanov, S.Y., Seryozhnikov, S.Y.: Parallel CPU- and GPU-algorithms for inverse problems in nondestructive testing. *Lobachevskii Journal of Mathematics* **39**(4), 486–493 (2018). <https://doi.org/10.1134/S1995080218040030>
2. Beilina, L., Klivanov, M.V., Kokurin, M.Y.: Adaptivity with relaxation for ill-posed problems and global convergence for a coefficient inverse problem. *J. Math. Sci.* **167**(3), 279–325 (may 2010). <https://doi.org/10.1007/s10958-010-9921-1>
3. Boehm, C., Martiartu, N.K., Vinard, N., Balic, I.J., Fichtner, A.: Time-domain spectral-element ultrasound waveform tomography using a stochastic quasi-newton method. *Proc. SPIE 10580, Medical Imaging 2018: Ultrasonic Imaging and Tomography* p. 105800H (03 2018). <https://doi.org/10.1117/12.2293299>
4. Goncharsky, A.V., Romanov, S.Y., Seryozhnikov, S.Y.: A computer simulation study of soft tissue characterization using low-frequency ultrasonic tomography. *Ultrasonics* **67**, 136–150 (apr 2016). <https://doi.org/10.1016/j.ultras.2016.01.008>
5. Goncharsky, A.V., Romanov, S.Y., Seryozhnikov, S.Y.: Supercomputer technologies in tomographic imaging applications. *Supercomputing Frontiers and Innovations* **3**(1), 41–66 (2016). <https://doi.org/10.14529/jsfi160103>
6. Goncharsky, A.V., Romanov, S.Y., Seryozhnikov, S.Y.: Low-frequency three-dimensional ultrasonic tomography. *Doklady Physics* **61**(5), 211–214 (may 2016). <https://doi.org/10.1134/s1028335816050086>
7. Goncharsky, A.V., Seryozhnikov, S.Y.: The architecture of specialized GPU clusters used for solving the inverse problems of 3D low-frequency ultrasonic tomography. In: Voevodin, V., Sobolev, S. (eds.) *Supercomputing. RuSCDays 2017. Communications in Computer and Information Science*. vol. 793, pp. 363–395. Springer, Cham. (2017)
8. Goncharsky, A.V., Romanov, S.Y.: Supercomputer technologies in inverse problems of ultrasound tomography. *Inverse Probl.* **29**(7), 075004 (2013). <https://doi.org/10.1088/0266-5611/29/7/075004>
9. Goncharsky, A.V., Romanov, S.Y.: Inverse problems of ultrasound tomography in models with attenuation. *Phys. Med. Biol.* **59**(8), 1979–2004 (apr 2014). <https://doi.org/10.1088/0031-9155/59/8/1979>
10. Goncharsky, A.V., Romanov, S.Y.: Iterative methods for solving coefficient inverse problems of wave tomography in models with attenuation. *Inverse Probl.* **33**(2), 025003 (jan 2017). <https://doi.org/10.1088/1361-6420/33/2/025003>
11. Goncharsky, A., Romanov, S., Seryozhnikov, S.: Inverse problems of 3D ultrasonic tomography with complete and incomplete range data. *Wave Motion* **51**(3), 389–404 (apr 2014). <https://doi.org/10.1016/j.wavemoti.2013.10.001>

12. Jirik, R., Peterlik, I., Ruiter, N., Fousek, J., Dapp, R., Zapf, M., Jan, J.: Sound-speed image reconstruction in sparse-aperture 3-D ultrasound transmission tomography. *IEEE T. Ultrason. Ferr.* **59**(2), 254–264 (feb 2012)
13. Klibanov, M.V., Timonov, A.A.: Carleman Estimates for Coefficient Inverse Problems and Numerical Applications. Walter de Gruyter GmbH (jan 2004)
14. Kuzhuget, A.V., Beilina, L., Klibanov, M.V., Sullivan, A., Nguyen, L., Fiddy, M.A.: Blind backscattering experimental data collected in the field and an approximately globally convergent inverse algorithm. *Inverse Probl.* **28**(9), 095007 (2012). <https://doi.org/10.1088/0266-5611/28/9/095007>
15. Mu, S.Y., Chang, H.W.: Dispersion and local-error analysis of compact LFE-27 formulas for obtaining sixth-order accurate numerical solutions of 3D Helmholtz equation. *Pr. Electromagn. Res. S.* **143**, 285–314 (2013)
16. Natterer, F.: Possibilities and limitations of time domain wave equation imaging. In: *AMS Vol.559: Tomography and Inverse Transport Theory*, pp. 151–162. American Mathematical Society (2011). <https://doi.org/10.1090/conm/559>
17. Natterer, F.: Sonic imaging. In: *Handbook of Mathematical Methods in Imaging*, pp. 1–23. Springer Nature (2014)
18. Romanov, S.: Optimization of numerical algorithms for solving inverse problems of ultrasonic tomography on a supercomputer. In: Voevodin, V., Sobolev, S. (eds.) *Supercomputing. RuSCDays 2017. Communications in Computer and Information Science*. vol. 793, pp. 67–79. Springer, Cham. (2017)
19. Sadovnichy, V., Tikhonravov, A., Voevodin, V., Opanasenko, V.: "Lomonosov": Supercomputing at Moscow State University. In: *Contemporary High Performance Computing: From Petascale toward Exascale*, p. 283307. Chapman & Hall/CRC Computational Science., Boca Raton, USA, CRC Press (2013)
20. Saha, R.K., Sharma, S.K.: Validity of a modified Born approximation for a pulsed plane wave in acoustic scattering problems. *Phys. Med. Biol.* **50**(12), 2823 (2005)
21. Sak, M., Duric, N., Littrup, P., Bey-Knight, L., Ali, H., Vallieres, P., Sherman, M.E., Gierach, G.L.: Using speed of sound imaging to characterize breast density. *Ultrasound Med. Biol.* **43**(1), 91–103 (jan 2017)
22. Schmidt, S., Duric, N., Li, C., Roy, O., Huang, Z.F.: Modification of Kirchhoff migration with variable sound speed and attenuation for acoustic imaging of media and application to tomographic imaging of the breast. *Med. Phys.* **38**(2), 998–1007 (jan 2011). <https://doi.org/10.1118/1.3539552>
23. Wiskin, J.W., Borup, D.T., Iuanow, E., Klock, J., Lenox, M.W.: 3-D nonlinear acoustic inverse scattering: Algorithm and quantitative results. *EEE Trans. Ultrason. Ferroelectr. Freq. Control* **64**(8), 1161–1174 (2017)
24. Zeqiri, B., Baker, C., Alosa, G., Wells, P.N.T., Liang, H.D.: Quantitative ultrasonic computed tomography using phase-insensitive pyroelectric detectors. *Phys. Med. Biol.* **58**(15), 5237 (2013). <https://doi.org/10.1088/0031-9155/58/15/5237>